A High-Integrity and Efficient GPS Integer Ambiguity Resolution Method

M. F. ABDEL-HAFEZ, Y. J. LEE, W. R. WILLIAMSON, J. D. WOLFE, and J. L. SPEYER
University of California-Los Angeles, Los Angeles, California

Received February 2003; Revised August 2003

ABSTRACT: *An efficient method for obtaining the admissible integer ambiguity hypotheses within a probabilistic volume is combined with an integer hypothesis testing method to reduce the convergence time to the GPS carrier-phase integers with high probability. The baseline coordinates, float ambiguities, and their covariance matrices are first estimated using a Kalman filter. To reduce the hypothesis set, the covariance matrix decorrelation method, which is the major contribution of the least-squares ambiguity decorrelation adjustment (LAMBDA) method, is then applied. The reduced admissible hypotheses are tested by the multiple-hypothesis Wald sequential probability test (MHWSPT) to select, with a given probability, the most likely hypothesis. This method considerably reduces the computational time needed to solve the integer ambiguity resolution problem at each epoch.*

NOMENCLATURE

ρ_i^k	k-th satellite code measurement at receiver i
$\dot{\rho}_i^k$	Doppler measurement between satellite k and receiver i
ϕ_i^k	k-th satellite carrier-phase measurement at receiver i
$\dot{\phi}_i^k$	Doppler shift between satellite k and receiver i
N_i^k	k-th satellite initial integer number of wavelengths from receiver i (integer ambiguity)
$\mathbf{x}^k$	k-th satellite position vector
$\mathbf{x}_i$	i-th receiver position vector (vehicle's position)
λ	carrier-phase wave length
c	speed of light in vacuum
τ^k	k-th satellite clock delay
$\dot{\tau}^k$	k-th satellite clock drift
τ_i	i-th receiver clock delay
$\dot{\tau}_i$	i-th receiver clock drift
I^k	k-th satellite ionospheric delay
T^k	k-th satellite tropospheric delay
E^k	k-th satellite transmitted ephemeris set error
MP_i^k	k-th satellite code multipath error at receiver i
mp_i^k	k-th satellite carrier multipath error at receiver i
η_i^k	code receiver noise
β_i^k	carrier-phase receiver noise
γ_i^k	Doppler measurement noise

INTRODUCTION

A wide range of applications of GPS require achieving centimeter-level accuracy. For those applications, GPS carrier-phase measurements must be used. Therefore, fast and reliable methods have been developed for resolving the carrier-phase integer ambiguity. Once this ambiguity has been resolved, the carrier-phase measurement acts like a high-accuracy GPS code measurement.

Most of the schemes in the literature start with treating the integer ambiguity as a float. After generating an initial estimate of the integer using the GPS code measurement, a hypothesis space is set, and the integer ambiguity is determined using a χ^2 test [1–3]. These algorithms all lack a proof of convergence. More theoretically involved algorithms that treat the integer ambiguity as a random integer vector can be found in [4] and [5]. Currently, real-time results are not available for these algorithms.

One of the most widely used methods for GPS integer ambiguity resolution is the least-squares ambiguity decorrelation adjustment (LAMBDA) method [6–8]. The LAMBDA method has been found to be quite efficient in processing data in the float estimation and using a transformation that preserves the probability volume. The heuristic aspect of the procedure is in resolving the integer from the float process. On the other hand, the multiple-hypothesis Wald sequential probability test (MHWSPT) [9–11] has been found to be a very efficient method for converging to the correct integers. This method is essentially a nonlinear sequential filter that, after conditioning of the measurements, is optimal.

We show here how these two methods can be combined such that a very efficient and accurate scheme results. The essential approach is to use the ambiguity covariance matrix decorrelation process of the LAMBDA method to effectively reduce the number of hypotheses. These hypotheses are then tested using the MHWSPT. A summary of the procedures for the proposed method is as follows:

1. Using a Kalman filter, the baseline coordinates, float ambiguities, and their covariance matrices are estimated as initial values.
2. The original ambiguity space is transformed into the approximately decorrelated one using the decorrelation transformation based on the ambiguity covariance matrix decorrelation that preserves the integer nature of the ambiguity.
3. The integer ambiguity searching set in the transformed integer ambiguity space is constructed, and the set is retransformed back to the original ambiguity space. A new hypothesis set, which is largely reduced compared with the original one, is constructed in the original space.
4. The MHWSPT is performed on the new set of hypotheses, and the integer ambiguity is resolved.

Considering a two-dimensional integer ambiguity problem, Figure 1 shows a schematic diagram for steps 1 through 3 of the proposed method. Figure 1(a) shows the ellipse defined by the float integer covariance matrix with a dashed box surrounding the integer hypotheses that need to be tested to obtain the correct integer ambiguity. The large correlations between the float integers that are indicated by this highly elongated ellipse explain why it is difficult to define a small integer hypothesis space. By transforming the original space in Figure 1(a) to a decorrelated space as in Figure 1(b), it becomes easy to obtain a compact hypothesis set, as seen in the small-sized dashed box of Figure 1(b). This small hypothesis space is transformed back to the original space as shown in Figure 1(c). At this last stage, and with this small-sized hypothesis space, the MHWSPT is conducted to fix the integer ambiguity by sequentially processing a uniquely formed measurement residual given these hypotheses.

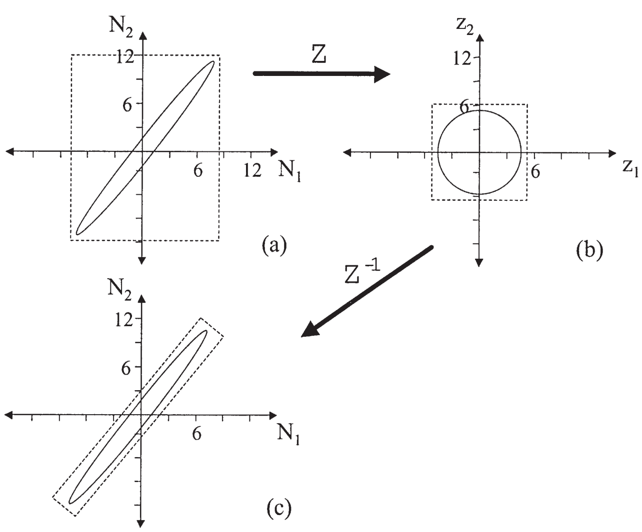

Fig. 1–Schematic Flow of Integer Ambiguity Space Transformations

The major contribution of the proposed method is that the reduced hypothesis set obtained from the covariance matrix decorrelation increases the efficiency and reliability of the algorithm while retaining the proven convergence criteria. Numerical examples provided at the end of the paper show the efficiency of the proposed method.

GPS OBSERVABLES

GPS receivers provide several types of GPS measurements. These measurements include coarse/acquisition (C/A)-code–derived pseudorange measurements, P-code–derived pseudorange measurements, carrier-phase measurements, and Doppler measurements. The latter three can be measured on two carrier frequencies—L1 and L2. The GPS receivers also provide, at a much lower frequency, the ephemeris data from which we extract the positions of the GPS satellites. The code measurement of satellite vehicle k by receiver i can be represented as

$$\rho_i^k = \left\|\mathbf{x}_i - \mathbf{x}^k\right\| + c\tau^k + c\tau_i + I^k + T^k + E^k + MP_i^k + \eta_i^k \tag{1}$$

while the carrier-phase measurement is represented as

$$\lambda(\phi_i^k + N_i^k) = \left\|\mathbf{x}_i - \mathbf{x}^k\right\| + c\tau^k + c\tau_i - I^k + T^k + E^k + mp_i^k + \beta_i^k \tag{2}$$

Similarly, the Doppler measurement between satellite vehicle k and receiver i is described as

$$\dot{\rho}_i^k = \dot{\phi}_i^k + c\dot{\tau}^k + c\dot{\tau}_i + \gamma_i^k \tag{3}$$

For a particular satellite, when the GPS measurement at the slave vehicle, subscript s, is differenced from the GPS measurement at a base vehicle in close proximity, subscript b, the common-mode errors are removed (these include I^k, T^k, E^k, $c\tau^k$, $c\dot{\tau}^k$). This is the single-differenced measurement that can be obtained for all satellites in view. By differencing two single-differenced measurements—for example, the single-differenced measurement of satellite 1 from that of satellite k—we remove the receiver clock bias and the receiver clock drift from the estimation problem. Thus, the following double-differenced code, carrier-phase, and Doppler measurement equations are obtained:

$$\nabla\Delta\rho^{k1} = \|\mathbf{x}_b - \mathbf{x}^k\| - \|\mathbf{x}_s - \mathbf{x}^k\| - (\|\mathbf{x}_b - \mathbf{x}^1\| - \|\mathbf{x}_s - \mathbf{x}^1\|) + \nabla\Delta\eta \tag{4}$$

$$\lambda(\nabla\Delta\phi^{k1} + \nabla\Delta N^{k1}) = \left\|\mathbf{x}_b - \mathbf{x}^k\right\| - \left\|\mathbf{x}_s - \mathbf{x}^k\right\| - \left(\left\|\mathbf{x}_b - \mathbf{x}^l\right\| - \left\|\mathbf{x}_s - \mathbf{x}^l\right\|\right) + \Delta\nabla\beta \tag{5}$$

$$\nabla\Delta\dot{\rho}^{k1} = \dot{\phi}_b^k - \dot{\phi}_s^k - (\dot{\phi}_b^1 - \dot{\phi}_s^1) + \nabla\Delta\gamma \tag{6}$$

Note that we assume the multipath error to be negligible. Here we seek to resolve the integer ambiguity $\nabla\Delta N^{k1}$ for all satellites k, $k \neq 1$, in view. We then linearize these equations about a nominal base and slave trajectories and stack all satellites' double-differenced measurements in vector form to obtain

$$\nabla\Delta\boldsymbol{\rho} = \nabla\Delta\bar{\boldsymbol{\rho}} + \Delta\mathbf{H}\Delta\delta\mathbf{x} + \nabla\Delta\boldsymbol{\eta} \tag{7}$$

$$\lambda(\nabla\Delta\boldsymbol{\phi} + \nabla\Delta\mathbf{N}) = \nabla\Delta\bar{\boldsymbol{\rho}} + \Delta\mathbf{H}\Delta\delta\mathbf{x} + \nabla\Delta\boldsymbol{\beta} \tag{8}$$

$$\nabla\Delta\dot{\boldsymbol{\rho}} = \nabla\Delta\dot{\bar{\boldsymbol{\rho}}} + \Delta\mathbf{H}\Delta\delta\dot{\mathbf{x}} + \nabla\Delta\boldsymbol{\gamma} \tag{9}$$

where $\Delta\mathbf{H}$ is the differenced linearization matrix that represents the receiver–satellite geometry. The unknowns in the above equations are $\nabla\Delta\mathbf{N}$, $\Delta\delta\mathbf{x}$, and $\Delta\delta\dot{\mathbf{x}}$. To make the integer ambiguity resolution scheme converge more rapidly, we generally combine the L1 and L2 measurements into a "widelane" measurement with a longer wavelength. Nevertheless, the proposed method was used only for L1 GPS integer ambiguity resolution, as will be shown in the experimental results.

KALMAN FILTER FOR FLOAT SOLUTION

We use a Kalman filter to generate an initial estimate of the integer ambiguity without enforcing the integer nature of the ambiguities. This is what is referred to in the literature as the float integer ambiguity. The filter utilizes both the double-differenced code measurement and the double-differenced carrier-phase measurement. We also use the double-differenced Doppler measurement to enhance the estimation accuracy, since it is a very clean signal in comparison with the code measurement.

Therefore, the state of the float filter includes the relative distance between the two receivers ($\Delta\mathbf{x}$), the float integer ambiguity ($\mathbf{N}$), and the relative velocity between the two receivers ($\Delta\dot{\mathbf{x}}$). Note that, from this point on, we denote $\mathbf{N} \equiv \nabla\Delta\mathbf{N}$ for short. Thus, the dynamic equations are described as

$$\underbrace{\begin{bmatrix} \Delta\dot{\mathbf{x}} \\ \dot{\mathbf{N}} \\ \Delta\ddot{\mathbf{x}} \end{bmatrix}}_{\dot{\mathbf{X}}(t)} = \underbrace{\begin{bmatrix} \mathbf{0} & \mathbf{0} & \mathbf{I} \\ \mathbf{0} & \mathbf{0} & \mathbf{0} \\ \mathbf{0} & \mathbf{0} & \mathbf{0} \end{bmatrix}}_{\mathbf{A}(t)} \underbrace{\begin{bmatrix} \Delta\mathbf{x} \\ \mathbf{N} \\ \Delta\dot{\mathbf{x}} \end{bmatrix}}_{\mathbf{X}(t)} + \underbrace{\begin{bmatrix} \mathbf{0} \\ \boldsymbol{\omega}_N \\ \boldsymbol{\omega}_V \end{bmatrix}}_{\mathbf{w}} \tag{10}$$

where the process noises $\boldsymbol{\omega}_N$ and $\boldsymbol{\omega}_V$ are used as filter-tuning parameters; $\boldsymbol{\omega}_N$ keeps the filter open during the state propagation; and $\boldsymbol{\omega}_V$ models the relative distance acceleration. By defining

$$\nabla\Delta\tilde{\boldsymbol{\phi}}(k) = \nabla\Delta\boldsymbol{\phi}(k) - \frac{\nabla\Delta\bar{\boldsymbol{\rho}}(k)}{\lambda}$$

$$\nabla\Delta\tilde{\boldsymbol{\rho}}(k) = \nabla\Delta\boldsymbol{\rho}(k) - \nabla\Delta\bar{\boldsymbol{\rho}}(k)$$

$$\nabla\Delta\dot{\tilde{\boldsymbol{\rho}}}(k) = \nabla\Delta\dot{\boldsymbol{\rho}}(k) - \nabla\Delta\dot{\bar{\boldsymbol{\rho}}}(k)$$

The linearized measurement equations for the three measurements become

$$\underbrace{\begin{bmatrix} \nabla\Delta\tilde{\boldsymbol{\rho}} \\ \nabla\Delta\tilde{\boldsymbol{\phi}} \\ \nabla\Delta\dot{\tilde{\boldsymbol{\rho}}} \end{bmatrix}}_{\mathbf{y}(t)} = \underbrace{\begin{bmatrix} \Delta\mathbf{H} & \mathbf{0} & \mathbf{0} \\ \mathbf{0} & -\mathbf{I} & \mathbf{0} \\ \mathbf{0} & \mathbf{0} & \Delta\mathbf{H} \end{bmatrix}}_{\mathbf{C}(t)} \begin{bmatrix} \Delta\mathbf{x} \\ \mathbf{N} \\ \Delta\dot{\mathbf{x}} \end{bmatrix} + \underbrace{\begin{bmatrix} \nabla\Delta\boldsymbol{\eta} \\ \dfrac{\nabla\Delta\boldsymbol{\beta} - \nabla\Delta\boldsymbol{\eta}}{\lambda} \\ \nabla\Delta\boldsymbol{\gamma} \end{bmatrix}}_{\mathbf{v}(t)} \tag{11}$$

We also linearize the slave measurement equation around the base position, such that

$$\Delta\delta\mathbf{x} \equiv \Delta\mathbf{x} = \mathbf{x}_b - \mathbf{x}_s$$

This approach is valid when the base and slave receivers are in close proximity, say, a few kilometers.

An estimate of the baseline, float ambiguity, and relative velocity is obtained using a Kalman filter of the form

$$\dot{\hat{\mathbf{X}}}(t) = \mathbf{A}(t)\hat{\mathbf{X}}(t) + \mathbf{P}(t)\mathbf{C}^T(t)\mathbf{V}(t)^{-1} \times \left[\mathbf{y}(t) - \mathbf{C}(t)\hat{\mathbf{X}}(t)\right] \tag{12}$$

where the estimator error covariance $\mathbf{P}(t)$ is given as

$$\dot{\mathbf{P}}(t) = \mathbf{A}(t)\mathbf{P}(t) + \mathbf{P}(t)\mathbf{A}^T(t) - \mathbf{P}(t)\mathbf{C}^T(t)V^{-1}(t)\mathbf{C}(t)\mathbf{P}(t) + \mathbf{W} \tag{13}$$

the covariance $\mathbf{P}(t)$ is explicitly decomposed as

$$\mathbf{P}(t) = \begin{bmatrix} \mathbf{Q}_{\hat{x}} & \mathbf{Q}_{\hat{x}\hat{N}} & \mathbf{Q}_{\hat{x}\hat{V}} \\ \mathbf{Q}_{\hat{x}\hat{N}} & \mathbf{Q}_{\hat{N}} & \mathbf{Q}_{\hat{N}\hat{V}} \\ \mathbf{Q}_{\hat{x}\hat{V}} & \mathbf{Q}_{\hat{N}\hat{V}} & \mathbf{Q}_{\hat{V}} \end{bmatrix} \tag{14}$$

and $\mathbf{V} = E[\mathbf{v}\mathbf{v}^T]$, $\mathbf{W} = E[\mathbf{w}\mathbf{w}^T]$, where E is the expectation operator.

Figures 2 through 6 show the results of the Kalman filter for a zero baseline experiment with the following experimental conditions:

- Place–rooftop of UCLA Engineering Building
- Receiver–Ashtech Z12
- Sampling rate–2 Hz

The baseline estimate is shown in Figure 2. The estimate converges to a small error within a short time span. This is a result of an accurate float integer ambiguity estimation as shown in Figure 3. An estimate of the relative velocity between the base and slave receivers is shown in Figure 4. Figures 5 and 6 show the diagonal elements of the covariance matrices of the baseline and integer ambiguity estimates, respectively. We are interested in the integer ambiguity estimate $\hat{N}$ and its corresponding covariance matrix, $\mathbf{Q}_{\hat{N}}$, which are used in the next section to determine the integer ambiguity hypotheses. The covariance matrix decorrelation algorithm of the LAMBDA method is used to construct a transformation that will assist in searching for integer ambiguity hypotheses in a certain hypothesis space defined by

$$(\hat{\mathbf{N}} - \mathbf{N})^T \mathbf{Q}_{\hat{N}}^{-1} (\hat{\mathbf{N}} - \mathbf{N}) \leq \chi^2 \tag{15}$$

for a statistically selected χ^2 value.

LAMBDA METHOD FOR DECORRELATING THE FLOAT INTEGER AMBIGUITY COVARIANCE MATRIX

The decorrelation of the covariance matrix $\mathbf{Q}_{\hat{N}}$ is constructed to simplify the minimization of the problem [6–8]

$$\min_{\mathbf{N}} \quad E\left\|\hat{\mathbf{N}} - \mathbf{N}\right\|^2_{\mathbf{Q}_{\hat{N}}^{-1}} \tag{16}$$

where $\hat{\mathbf{N}} \in R^n$ is the set of float vectors of order n, and $\mathbf{N} \in Z^n$ is the set of integer vectors of order n.

If the covariance matrix $\mathbf{Q}_{\hat{N}}$ is very precise in representing the uncertainty in the float integer ambiguity, then the above minimization problem should yield the true integer ambiguity. Because the float Kalman filter relaxes the constraint relating to the integer nature of the ambiguities, the float integer ambiguity covariance matrix may not always be accurate in representing the deviation of the float integer ambiguity from the true integer ambiguity. Hence, we instead use the minimization problem in equation (16) to obtain the most likely hypotheses. These hypotheses need to be tested through a method that will assign probability to the various hypotheses, and the hypothesis that is in fact the true integer ambiguity should have an associated probability that approaches 1. Only after this condition has been met is this hypothesis declared the true integer ambiguity.

To solve the minimization problem in equation (16), we first need to decorrelate the ambiguity covariance matrix $\mathbf{Q}_{\hat{N}}$ to try to eliminate the correlation between the transformed ambiguities. This minimization problem will be easier to solve in the new transformed space.

The decorrelation process transforms the unknown integer ambiguity variables into unknown innovation variables. Each innovation variable brings new information that is independent from the previous variables, thereby transforming the fully populated integer ambiguity covariance into a diagonal matrix that corresponds to the covariance of the

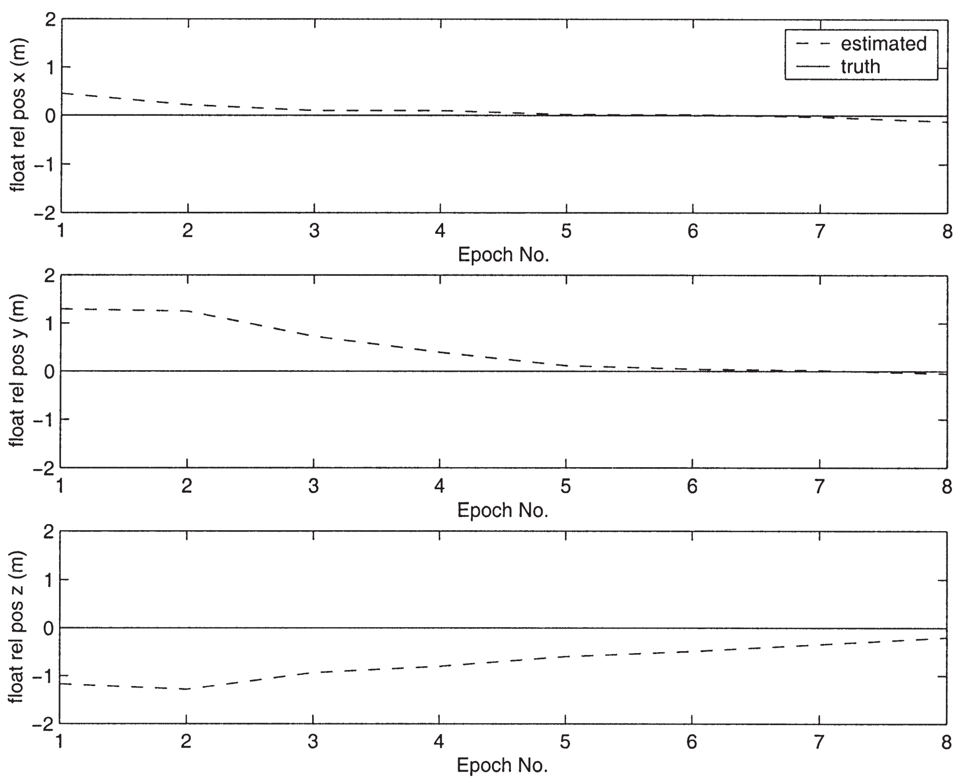

Fig. 2–Zero Baseline Estimate from the Kalman Filter

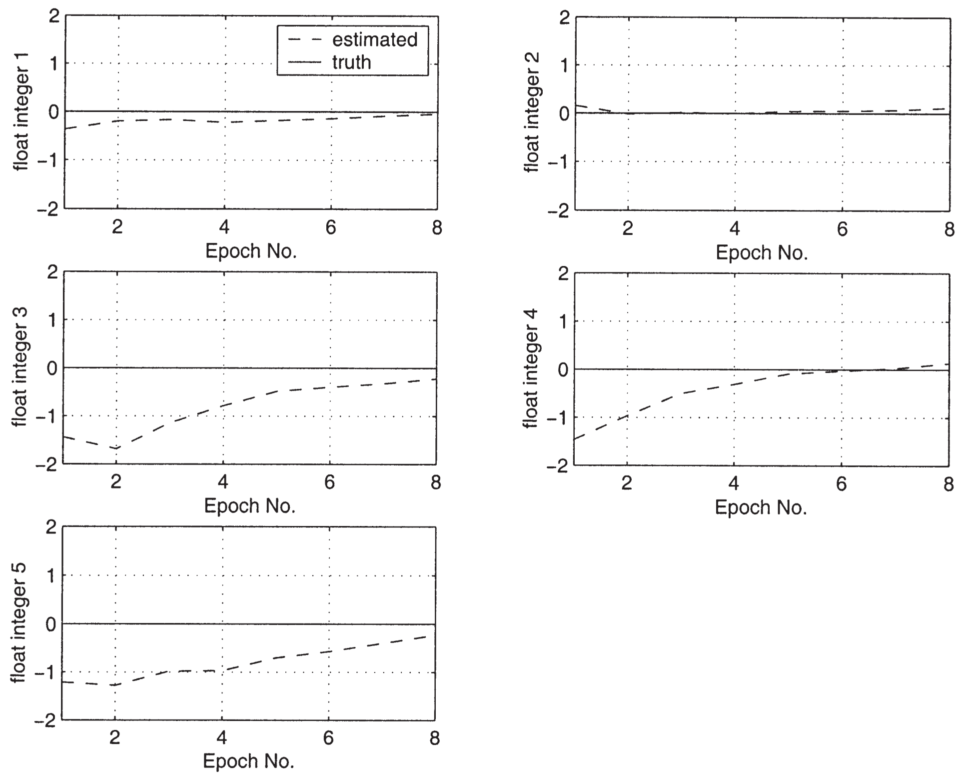

Fig. 3–Float Ambiguity Estimate from the Kalman Filter

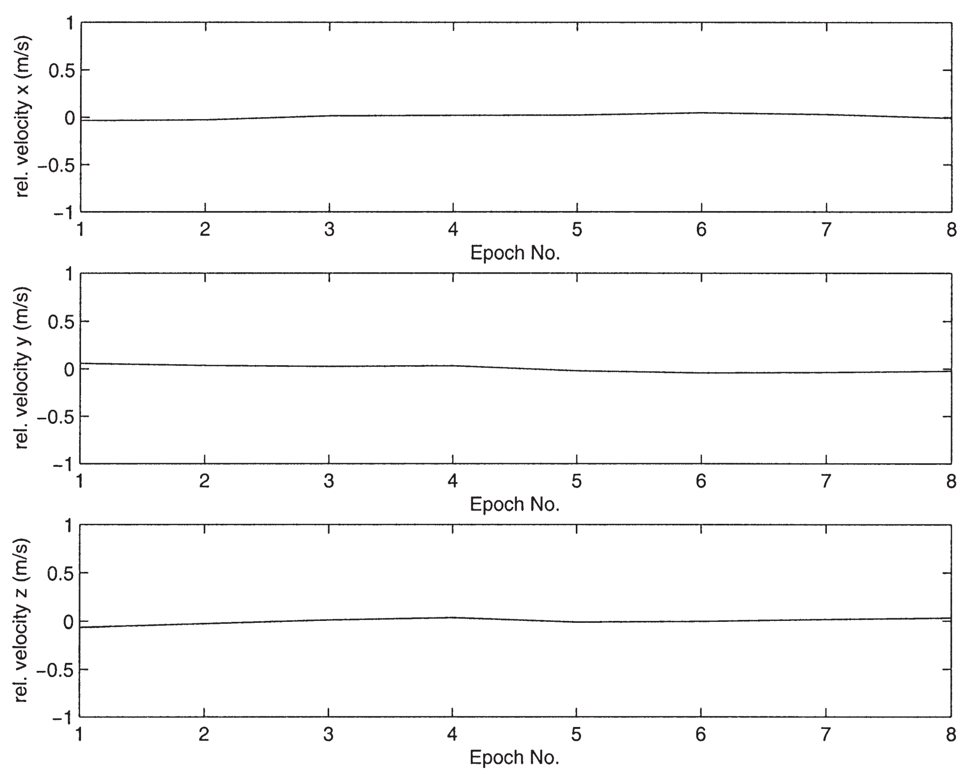

Fig. 4–Relative Velocity Estimate from the Kalman Filter

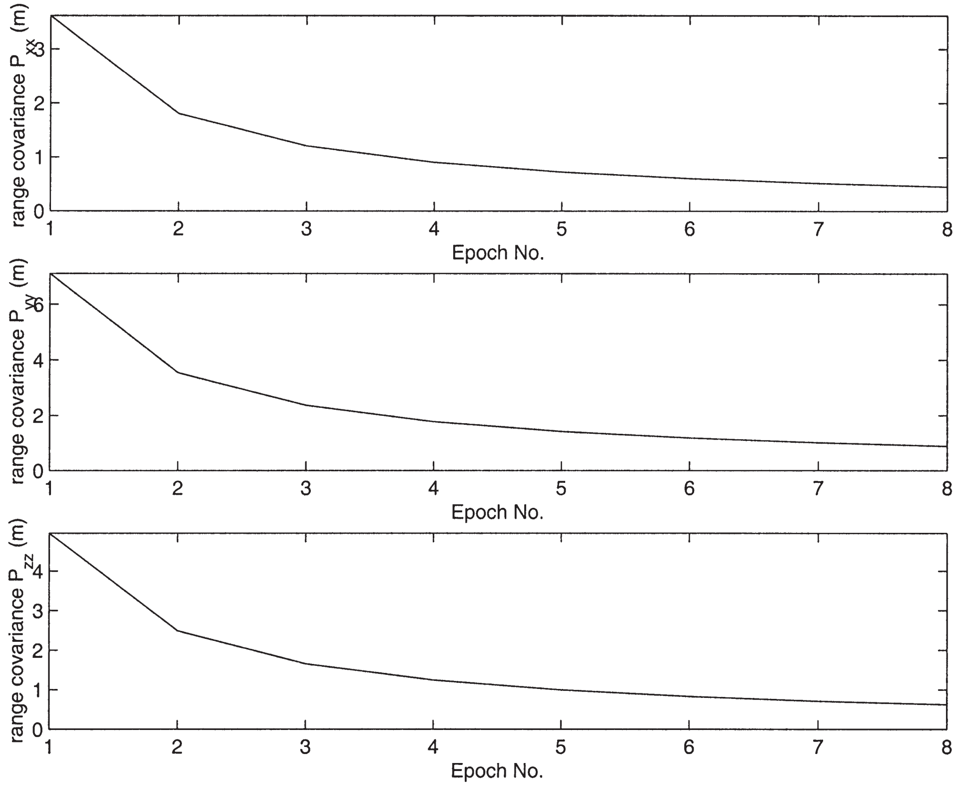

Fig. 5–Baseline Covariance from the Kalman Filter

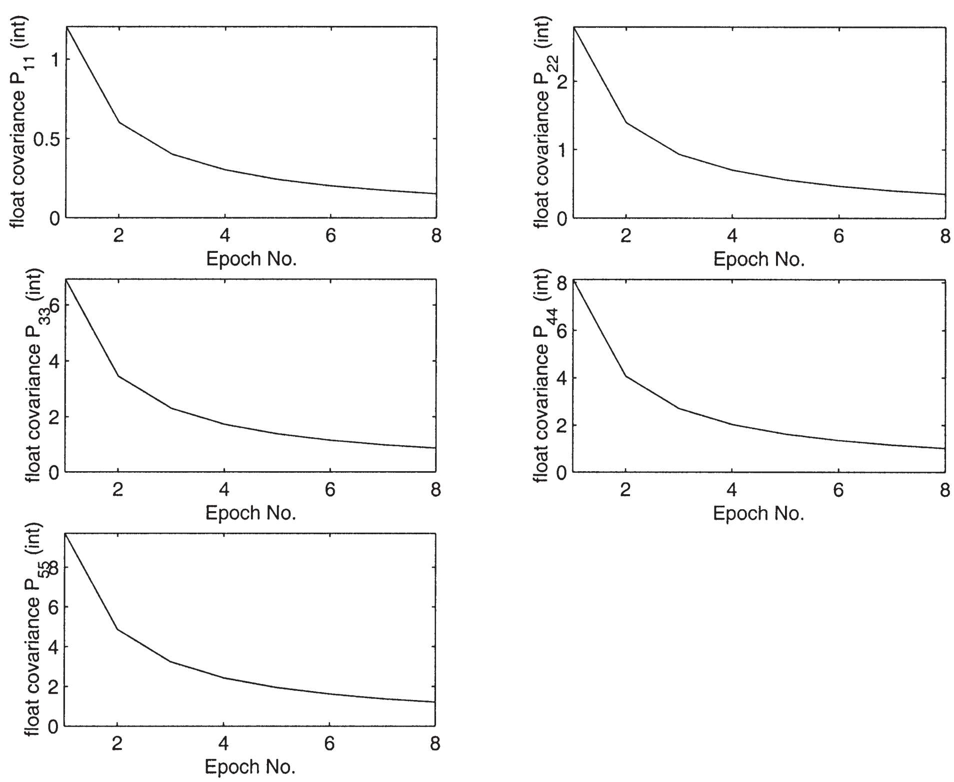

Fig. 6–Float Ambiguity Covariance from the Kalman Filter

innovation variables. This is done by introducing the conditional integer ambiguity transformation.

We note that for any two, possibly vector, variables $\mathbf{x}$ and $\mathbf{y}$, the conditional mean and covariance are defined as [12]

$$\mathbf{m_{x/y}} = \mathbf{m_x} + \mathbf{P_{xy}} \mathbf{P_{yy}^{-1}} (\mathbf{y} - \mathbf{m_y}) \tag{17}$$

$$\mathbf{P_{x/y}} = \mathbf{P_{xx}} - \mathbf{P_{xy}} \mathbf{P_{yy}^{-1}} \mathbf{P_{yx}} \tag{18}$$

respectively, where $\mathbf{m_x} \equiv E[\mathbf{x}]$, $\mathbf{m_{x/y}} \equiv E[\mathbf{x}|\mathbf{y}]$, $\mathbf{P_{xy}} \equiv E[(\mathbf{x}-\mathbf{m_x})\,(\mathbf{y}-\mathbf{m_y})^T]$, and $\mathbf{P}_{x/y} \equiv E[(\mathbf{x}-\mathbf{m_x})(\mathbf{x}-\mathbf{m_x})^T|\mathbf{y}]$. Thus, the transformed innovation variables are represented as follows:

$$z_1 = \hat{N}_{1/0} = \hat{N}_1 \tag{19}$$

$$\begin{aligned} z_2 = \hat{N}_{2/1} &= \hat{N}_2 + E\Big[(N_2 - \hat{N}_2)(N_1 - \hat{N}_1)\Big] \\ &\quad \Big[E[N_1 - \hat{N}_1]^2\Big]^{-1} (N_1 - \hat{N}_1) \\ &= \hat{N}_2 + \sigma_{\hat{N}_2,\hat{N}_1} \sigma_{\hat{N}_1}^{-2} (N_1 - \hat{N}_1) \end{aligned} \tag{20}$$

where $\mathbf{N} = [N_1, N_2, \ldots, N_n]^T$ and $\hat{\mathbf{N}} = [\hat{N}_1, \hat{N}_2, \ldots, \hat{N}_n]^T$. The covariance of the transformed innovation variables is given by

$$\sigma_{z_1}^2 = \sigma_{\hat{N}_1}^2 \tag{21}$$

$$\sigma_{z_2}^2 = \sigma_{\hat{N}_2}^2 - \sigma_{\hat{N}_2,\hat{N}_1} \sigma_{\hat{N}_1}^{-2} \sigma_{\hat{N}_2,\hat{N}_1} \tag{22}$$

$$\sigma_{z_2,z_1} = \sigma_{\hat{N}_2,\hat{N}_1} - \sigma_{\hat{N}_2,\hat{N}_1} = 0 \tag{23}$$

Note from equation (23) that there is no correlation between the transformed integer ambiguity z_1 and z_2. In the same way,

$$\begin{aligned} z_3 &= \hat{N}_{3/2,1} \equiv \hat{N}_{3/(2/1,1)} \\ &= \hat{N}_3 + E\Big[(N_3 - \hat{N}_3)\,[(N_{2/1} - \hat{N}_{2/1})\,(N_1 - \hat{N}_1)]\Big] \\ &\quad \times \begin{bmatrix} \sigma_{\hat{N}_{2/1}}^2 & 0 \\ 0 & \sigma_{\hat{N}_1}^2 \end{bmatrix}^{-1} \begin{bmatrix} N_{2/1} - \hat{N}_{2/1} \\ N_1 - \hat{N}_1 \end{bmatrix} \\ &= N_3 + \Big[\sigma_{\hat{N}_3,\hat{N}_{2/1}} \;\; \sigma_{\hat{N}_3,\hat{N}_1}\Big] \begin{bmatrix} \sigma_{\hat{N}_{2/1}}^2 & 0 \\ 0 & \sigma_{\hat{N}_1}^2 \end{bmatrix}^{-1} \begin{bmatrix} N_{2/1} - \hat{N}_{2/1} \\ N_1 - \hat{N}_1 \end{bmatrix} \\ &= \hat{N}_3 + \sigma_{\hat{N}_3,\hat{N}_{2/1}} \sigma_{\hat{N}_{2/1}}^{-2} (N_{2/1} - \hat{N}_{2/1}) \\ &\quad + \sigma_{\hat{N}_3,\hat{N}_1} \sigma_{\hat{N}_1}^{-2} (N_1 - \hat{N}_1) \end{aligned} \tag{24}$$

Again, z_3 is uncorrelated with z_1 and z_2. In general,

$$\hat{N}_{i/I} = \hat{N}_i + \sum_{j=1}^{i-1} \sigma_{\hat{N}_i,\hat{N}_{j/J}} \sigma_{\hat{N}_{j/J}}^{-2} (\hat{N}_{j/J} - N_j) \tag{25}$$

where $\hat{N}_{i/I} \equiv \hat{N}_{i/(i-1,i-2,\ldots,1)}$. Thus in matrix form, we obtain

$$\underbrace{\begin{bmatrix} \hat{N}_1 - N_1 \\ \hat{N}_2 - N_2 \\ \hat{N}_3 - N_3 \\ \vdots \end{bmatrix}}_{\hat{\mathbf{N}}-\mathbf{N}} = \underbrace{\begin{bmatrix} 1 & & & \\ \sigma_{\hat{N}_2,\hat{N}_1}\sigma_{\hat{N}_1}^{-2} & 1 & & \\ \sigma_{\hat{N}_3,\hat{N}_1}\sigma_{\hat{N}_1}^{-2} & \sigma_{\hat{N}_3,\hat{N}_{2/1}}\sigma_{\hat{N}_{2/1}}^{-2} & 1 & \\ & & & \ddots \end{bmatrix}}_{\mathbf{L}} \times \underbrace{\begin{bmatrix} \hat{N}_1 - N_1 \\ \hat{N}_{2/1} - N_2 \\ \hat{N}_{3/2,1} - N_3 \\ \vdots \end{bmatrix}}_{\hat{\mathbf{z}}-\mathbf{z}} \tag{26}$$

Therefore, the integer ambiguity covariance matrix may be decomposed in terms of $\mathbf{L}$ and $\mathbf{D}$ as

$$\mathbf{Q}_{\hat{N}} = E\Big[(\hat{\mathbf{N}} - \mathbf{N})\,(\hat{\mathbf{N}} - \mathbf{N})^T\Big] = \mathbf{LDL}^T \tag{27}$$

where $\mathbf{D} = \mathrm{diag}\,(\sigma_{\hat{N}_1}^2, \sigma_{\hat{N}_{2/1}}^2, \ldots, \sigma_{\hat{N}_{n/N}}^2)$.

Since the $\mathbf{LDL}^T$ transformation—$\mathbf{L}$ lower triangular with 1's on the diagonal—is unique, transforming $\mathbf{Q}_{\hat{N}}$ in this form will directly give the $\mathbf{L}$ and $\mathbf{D}$ matrices. This eliminates the need to hand-calculate the variance and covariance terms in the $\mathbf{L}$ and $\mathbf{D}$ matrices [7].

This conditional least-squares principle can be used to transform the integer ambiguity covariance matrix into a diagonal matrix by selecting $\mathbf{Z} = \mathbf{L}^{-1}$; thus

$$\hat{\mathbf{z}} = \mathbf{Z}\hat{\mathbf{N}}$$
$$\mathbf{Q}_{\hat{z}} = \mathbf{Z}\mathbf{Q}_{\hat{N}}\mathbf{Z}^T = \mathbf{D}$$

and the minimization problem of equation (16) can be represented in the transformed space as

$$\min_{\mathbf{Z}} \mathbf{E}\left\|\hat{\mathbf{z}} - \mathbf{z}\right\|_{\mathbf{Q}_{\hat{z}}}^2$$

While this transformation simplifies the search for best integer ambiguity candidates while preserving the volume of the search space, it does not preserve the integer nature of the ambiguities since the $\mathbf{L}^{-1}$ elements do not usually belong to the integer space, [6–8]. Also, since the transformation is based on conditional least squares, we need to ensure that the transformed integers are sorted such that the smallest covariance integers are conditioned first. For all these reasons, a special form of the Gaussian transformation that preserves the integer nature of the ambiguities is used for the ambiguity transformation based on the LAMBDA method [6–8].

Thus, after decorrelating the covariance matrix, we can easily and with small computational time determine the integer hypotheses that lie within a specified volume. We need to use a method that assigns a probabilistic measure for each of the hypotheses. Therefore, the MHWSPT is used to recursively determine the probability that each hypothesis is the correct integer ambiguity given the measurement history, as will be seen in the next section.

THE MULTIPLE HYPOTHESIS WALD SEQUENTIAL PROBABILITY TEST

This method was first introduced in [9]. Recently it was used in [11] for the problem of integer ambiguity resolution. The MHWSPT is a statistical method used for the validation of integer ambiguity. It blends both code and carrier-phase measurements to form a residual that is used to obtain the probability of a certain integer hypothesis being the correct integer ambiguity. While the carrier-phase measurements are sufficient for this method to converge on the correct integer ambiguity, combining them with the code measurements speeds up the method's convergence [11].

The residual is defined for the i-th integer hypothesis, $\mathbf{N}_i$, as follows:

$$\mathbf{r}(k) = \begin{bmatrix} \mathbf{r}^1(k) \\ \mathbf{r}^2(k) \end{bmatrix} = \tilde{\mathbf{E}}(k) \cdot \begin{bmatrix} \lambda \nabla\Delta\tilde{\boldsymbol{\phi}}(k) \\ \nabla\Delta\tilde{\boldsymbol{\rho}}(k) \end{bmatrix}$$
$$= \tilde{\mathbf{E}}(k) \cdot \begin{bmatrix} \nabla\Delta\boldsymbol{\beta} - \lambda\mathbf{N}_i + \nabla\mathbf{H}(k)\Delta\delta\mathbf{x}(k) \\ \nabla\mathbf{H}(k)\Delta\delta\mathbf{x}(k) + \nabla\Delta\boldsymbol{\eta} \end{bmatrix}$$
$$= \begin{bmatrix} -\lambda \cdot \mathbf{E}(k) \\ -\lambda \cdot \mathbf{I} \end{bmatrix} \mathbf{N}_i + \begin{bmatrix} \mathbf{E}(k) \cdot \nabla\Delta\boldsymbol{\beta} \\ \nabla\Delta\boldsymbol{\beta} - \nabla\Delta\boldsymbol{\eta} \end{bmatrix} \tag{28}$$

where $\tilde{\mathbf{E}}$, defined below for n double-differenced measurements, is a projection that eliminates the term associated with $\Delta\delta\mathbf{x}$

$$\tilde{\mathbf{E}} = \begin{bmatrix} \mathbf{E} & 0 \\ \mathbf{I}_{n\times n} & -\mathbf{I}_{n\times n} \end{bmatrix}^{(2n-3)\times 2n} \tag{29}$$

and $\mathbf{E}$ is the left annihilator of the single-differenced measurement matrix $\nabla\mathbf{H}$. The remaining residual is essentially an independent and identically distributed (iid) sequence for which the MHWSPT is theoretically suited. This iid measurement sequence has mean and covariance given by

$$\mathbf{m}(\mathbf{N}_i, k) = \begin{bmatrix} -\lambda \cdot \mathbf{E}(k) \cdot \mathbf{N}_i \\ -\lambda \cdot \mathbf{N}_i \end{bmatrix} \tag{30}$$

$$\tilde{\mathbf{V}}(k) = \tilde{\mathbf{E}}(k) \cdot \mathbf{V} \cdot \tilde{\mathbf{E}}(k)^T \tag{31}$$

respectively, where

$$\mathbf{V} = \begin{bmatrix} \mathbf{V}_{car.} & \mathbf{0}_{\mathbf{n}\times\mathbf{n}} \\ \mathbf{0}_{\mathbf{n}\times\mathbf{n}} & \mathbf{V}_{code} \end{bmatrix} \tag{32}$$

The MHWSPT [9, 11] recursively calculates the probability that each of the integer hypotheses under consideration is the correct integer ambiguity given the measurement sequence up to the current time, $F_i(k)$, $i = 1 \ldots m$. This is explicitly expressed as

$$F_i(k) = P(\mathbf{N}_i | \mathbf{r}_0, \mathbf{r}_1, \ldots, \mathbf{r}_k) \tag{33}$$

By Bayes' rule, this can be expressed as

$$F_i(k) = \frac{P(N_i, \mathbf{r}_k | \mathbf{r}_0, \mathbf{r}_1, \ldots, \mathbf{r}_{k-1})}{P(\mathbf{r}(k) | \mathbf{r}_0, \mathbf{r}_1, \ldots, \mathbf{r}_{k-1})} \tag{34}$$

Applying Bayes' rule to the numerator of equation (34), we obtain

$$P(\mathbf{N}_i, \mathbf{r}_k | \mathbf{r}_0, \mathbf{r}_1, \ldots, \mathbf{r}_{k-1}) = P(\mathbf{r}_k | \mathbf{N}_i, \mathbf{r}_0, \mathbf{r}_1, \ldots, \mathbf{r}_{k-1}) \times P(\mathbf{N}_i | \mathbf{r}_0, \mathbf{r}_1, \ldots, \mathbf{r}_{k-1}) \tag{35}$$

Since we assume that the measurement sequence is iid, we have

$$P(\mathbf{r}_k | \mathbf{N}_i, \mathbf{r}_0, \mathbf{r}_1, \ldots, \mathbf{r}_{k-1}) = P(\mathbf{r}_k | \mathbf{N}_i) \equiv f_i(\mathbf{r}(k)) \tag{36}$$

Therefore, by noting that

$$P(\mathbf{N}_i | \mathbf{r}_0, \mathbf{r}_1, \ldots, \mathbf{r}_{k-1}) = F_i(k-1) \tag{37}$$

we have

$$P(\mathbf{N}_i, \mathbf{r}_k | \mathbf{r}_0, \mathbf{r}_1, \ldots, \mathbf{r}_{k-1}) = f_i(\mathbf{r}(k)) \times F_i(k-1)$$

The numerator of equation (34) can be expressed as

$$P(\mathbf{r}(k) | \mathbf{r}_0, \mathbf{r}_1, \ldots, \mathbf{r}_{k-1}) = P(\mathbf{r}(k)) = \sum_{j=1}^{m} P(\mathbf{N}_j, \mathbf{r}_k | \mathbf{r}_0, \mathbf{r}_1, \ldots, \mathbf{r}_{k-1}) = \sum_{j=1}^{m} f_j(\mathbf{r}(k)) \times F_j(k-1) \tag{38}$$

Hence,

$$F_i(k) = \frac{F_i(k-1) \times f_i(\mathbf{r}(k))}{\sum_{j=1}^{m} F_j(k-1) \times f_j(\mathbf{r}(k))} \tag{39}$$

The probability density function of $\mathbf{r}(k)$ given any integer hypothesis $\mathbf{N}_i$, $f_i(\mathbf{r}(k))$ is calculated, assuming a Gaussian residual $\mathbf{r}(k)$, as

$$f_i(r(k)) = C \cdot \exp^{-\frac{1}{2}[\mathbf{r}_i(k) - \mathbf{m}(\mathrm{N}_{i,k})]^T \tilde{\mathbf{V}}^{-1}(k)[\mathbf{r}_i(k) - \mathbf{m}(\mathrm{N}_{i,k})]}$$

The set of possible integer hypotheses is determined by first averaging the code position estimate over some time period. This is called the float mode. The corresponding integer number of widelane wavelengths is then computed, denoted the base hypothesis. The possible set per double-differenced measurement is then computed by taking a number of integers around that value. After the set of all possible integer hypotheses has been determined, we initialize $F_i(0)$ (all integer hypotheses are usually set to be equally probable) and start sequentially propagating $F_i(k)$ at each GPS time epoch, k. This process is essentially a nonlinear filter. After some time, we note that all $F_i(k)$ are almost identically zero except for the correct integer hypothesis, which approaches 1. At the instant when a certain correct integer hypothesis threshold probability is met, we declare the corresponding hypothesis to be the true integer ambiguity.

THE LAMBDA-ASSISTED WALD TEST

When the MHWSPT was introduced in the previous section, the methodology for selecting the integer ambiguity hypotheses was discussed. It was noted that initially, the float integer estimator is performed for a number of epochs assumed sufficient for convergence. Then, the resulting float ambiguity is rounded to the nearest integer, denoted the base hypothesis. The integer hypotheses are selected by taking ± 2, or possibly more, integers around the base hypothesis for each satellite measurement integer ambiguity. This scheme produces a large number of integer hypotheses—for instance, 3,125 hypotheses when six satellites are in view. It is here where the LAMBDA covariance matrix decorrelation algorithm becomes very useful. The LAMBDA decorrelation algorithm is used to decorrelate the integer covariance matrix, thereby reducing the time needed to search for all possible hypotheses in the covariance matrix ellipsoidal volume represented in equation (15). Thus, a quick search for hypotheses with small χ_i^2 is performed such that $\chi_i^2 < \chi^2$ for each hypothesis i.

χ^2 is fixed to some value that will guarantee to a certain probability that the correct integer hypothesis is among the candidates enclosed by the covariance matrix ellipsoidal volume. This is equivalent to fixing the volume of the ellipsoidal region to a value that will guarantee the existence of a certain number of candidates within that volume. Checking the maximum χ_i^2 will indicate the probability of having the correct hypothesis in that volume.

Therefore, to be more certain that the covariance matrix ellipsoidal volume will enclose the true integer ambiguity, enough time is allowed for the Kalman filter to converge. At the same time, the ellipsoidal volume is enlarged to cover more hypotheses. Thus, the χ^2 value is fixed to obtain at least 100 candidates; for the hardware-in-the-loop simulation (HILSIM) experiment discussed below, $\chi^2 = 197.0$.

These hypotheses are then passed to the MHWSPT. The MHWSPT will sequentially update the probability that each integer hypothesis is the correct integer ambiguity given the measurement history up to the current time. Once a certain integer hypothesis probability is very close to 1.0, usually taken to be $F_i(k) > 0.999$, that integer hypothesis is declared the correct integer ambiguity. In the next section we present various real-time experimental results for the proposed method.

EXPERIMENTAL RESULTS

The algorithm was tested under various conditions and environments to verify its functionality. We show here results of a zero baseline test, static as well as dynamic car tests (2.31 m baseline), and a highly dynamic two-aircraft real-time simulation test (40 m baseline). While most results shown are for widelane GPS effective signals, the ability of the proposed algorithm to resolve L1 integer ambiguity is also verified through experimental results. The discussion that follows assumes use of widelane GPS measurements unless stated otherwise.

Figure 7 presents real-time results for a zero-baseline test. The figure shows the probability associated with 10 integer hypotheses out of a total of 100 hypotheses. The true hypothesis was hypothesis 8, and the MHWSPT detected it correctly when the corresponding probability exceeded the threshold probability. One can see that the probability associated with the correct hypothesis converged fairly quickly to approach 1.

Figure 8 presents the baseline estimation error after the integer ambiguity was fixed for the zero baseline experiment. The figure shows the expected high carrier-phase estimation accuracy due to the low-magnitude measurement noise. This is also a result of the elimination of the common-mode errors and receiver clock biases in the double-differenced carrier-phase measurement.

The algorithm was tested in a real environment by placing two receivers 2.31 m apart, fixed to the rooftop of a car. The range between the two receivers was estimated in real time when the car was static and when it was moving at a speed of around 30 km/h. In the latter test, the carrier-phase integer ambiguity resolution scheme was initiated after the start of the motion.

Figure 9 shows the probability of the various hypotheses being the correct integer ambiguity. As in the above zero baseline experiment, as well as in the experimental examples to follow, the probabilities associated with 10 out of a total 100 hypotheses are shown. It can be seen that the correct integer ambiguity was detected, but a longer convergence time was required in comparison with the zero baseline experiment. It can also be noted that the probability associated with the correct hypothesis (hypothesis 8) was not strictly increasing as a function of time. This result is most likely due to environmental GPS signal errors, such as small-magnitude multipath errors.

Figures 10 and 11, respectively, show the results of the carrier-phase–based range estimation for the static and dynamic car tests after the integer ambiguity had been resolved. It can be seen that the range error is close to zero mean. The deviation of the estimation error around the mean is within the double-differenced carrier-phase noise level.

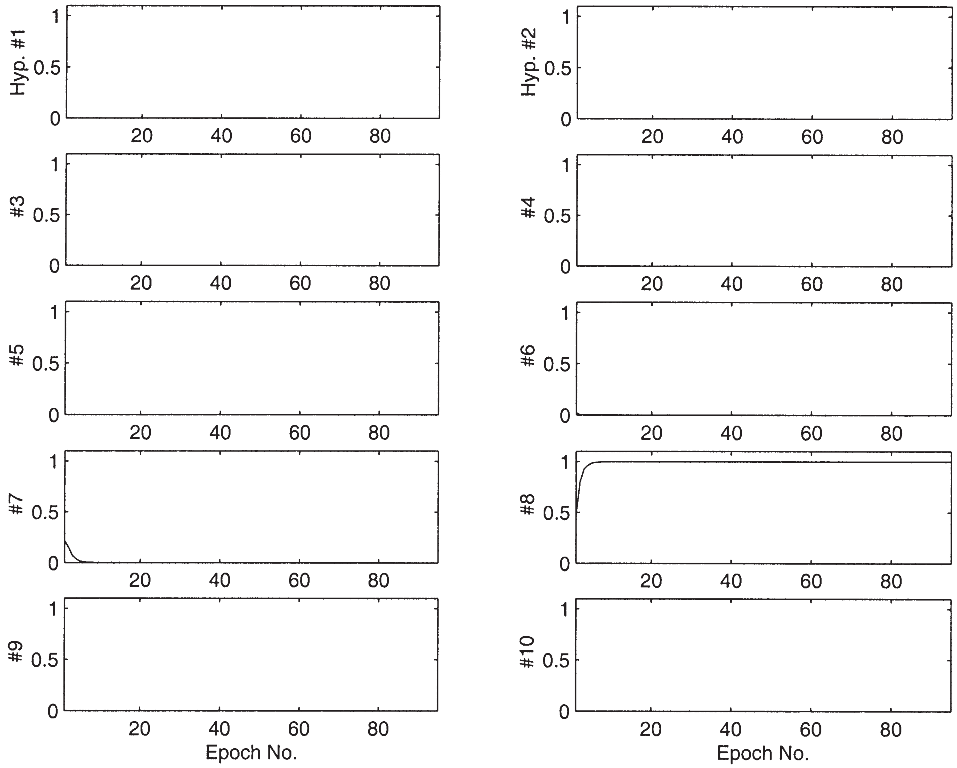

Fig. 7–MHWSPT Hypothesis Probabilities, Zero Baseline Experiment

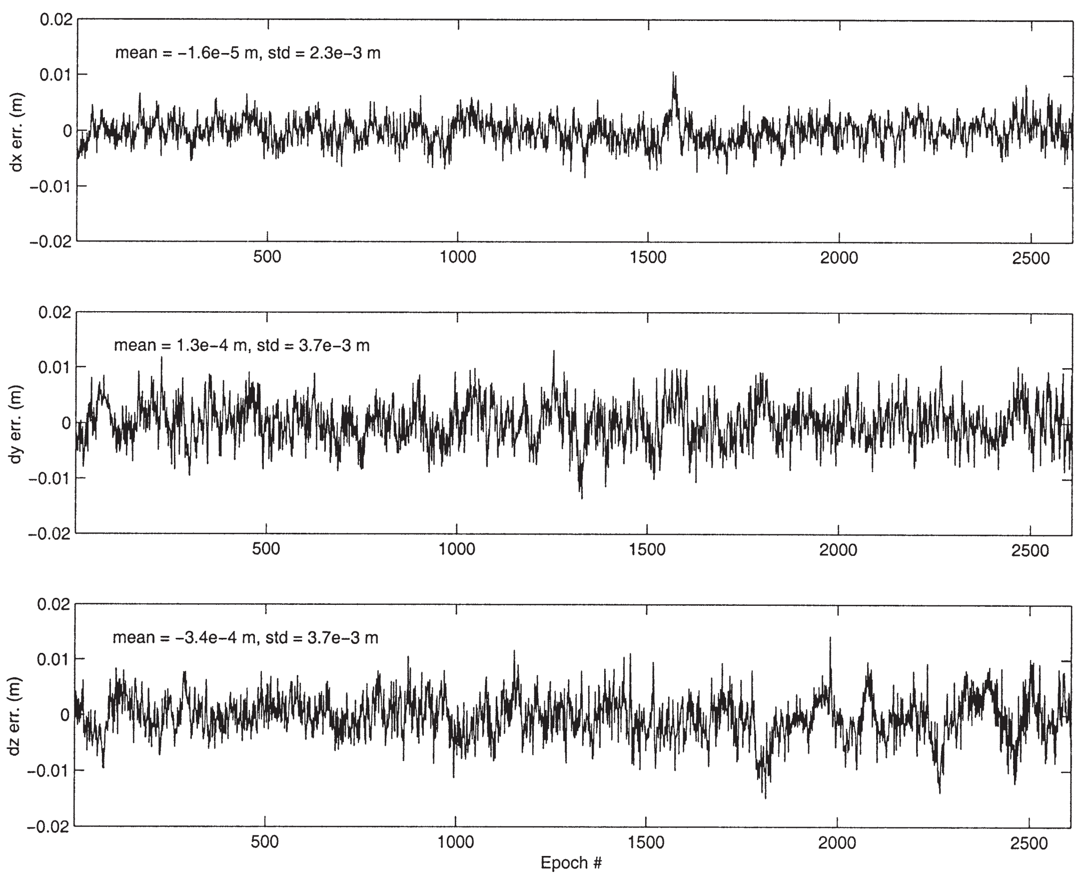

Fig. 8–Baseline Estimation Error after Fixing the Integers, Zero Baseline Experiment

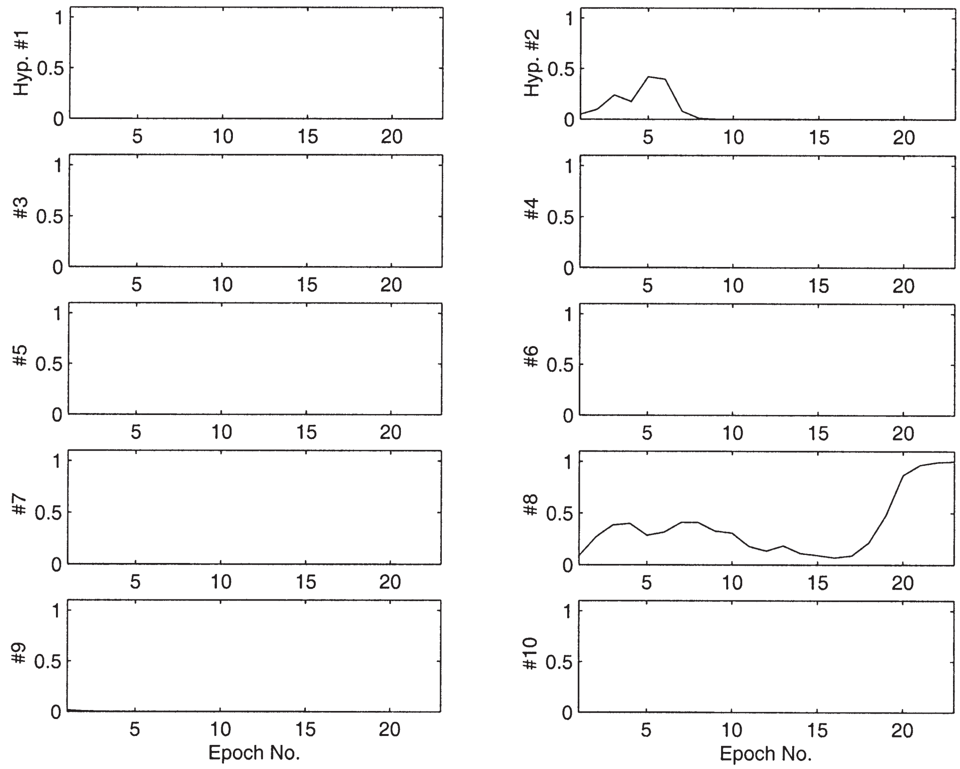

Fig. 9–MHWSPT Hypothesis Probabilities, Dynamic 2.31 m Baseline Car Test

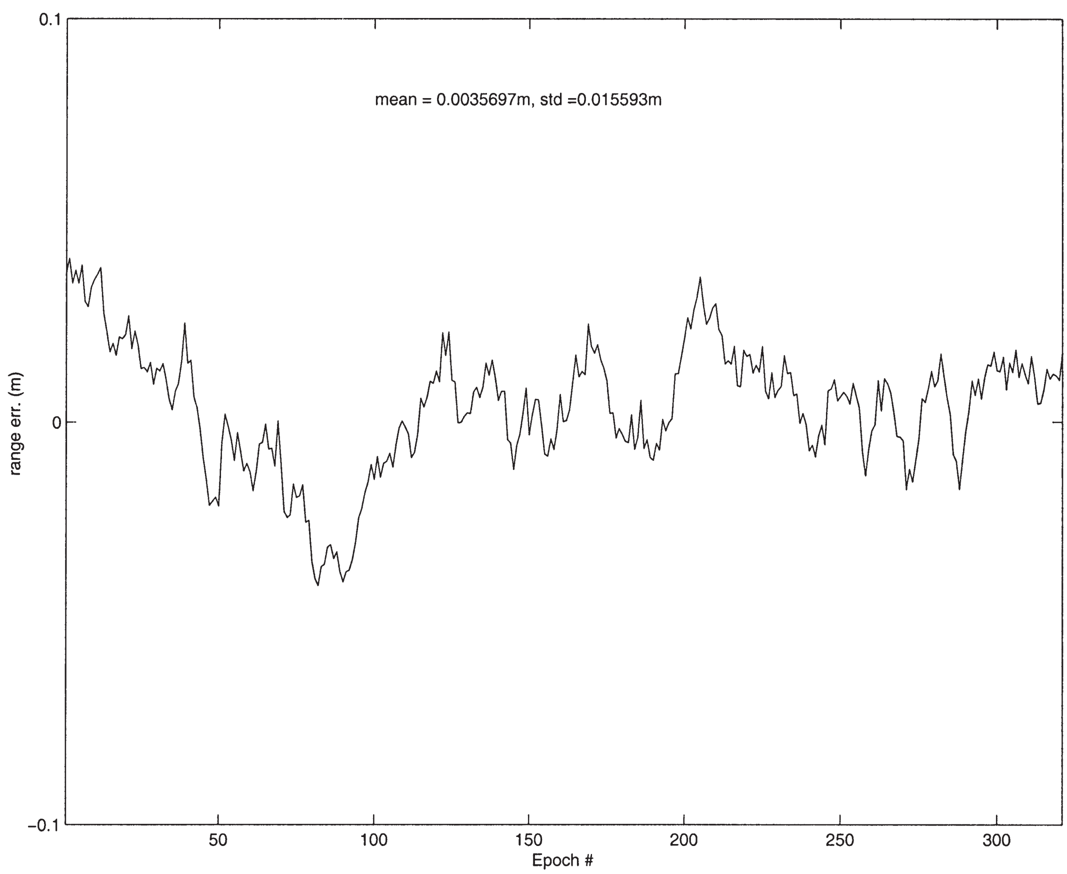

Fig. 10–Baseline Estimation Error after Fixing the Integers, Static 2.31 m Baseline Car Test

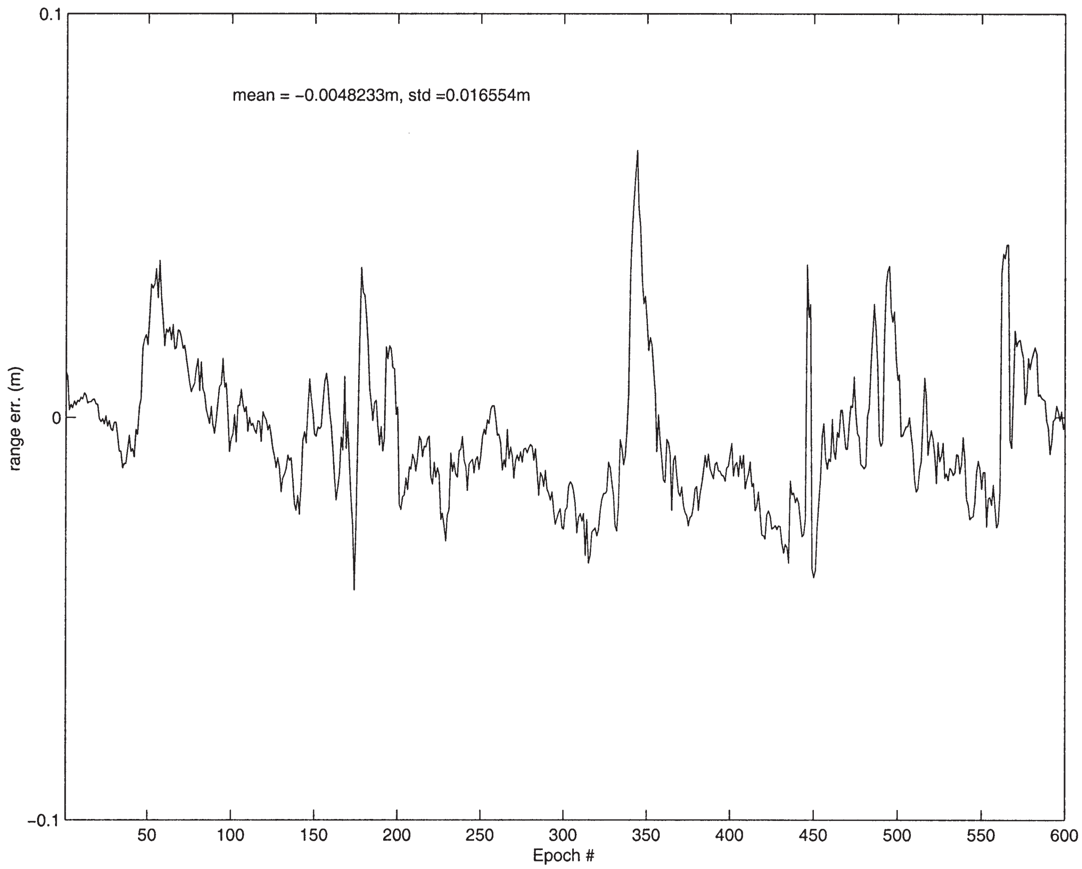

Fig. 11–Baseline Estimation Error after Fixing the Integers, Dynamic 2.31 m Baseline Car Test

The algorithm was also tested in a highly dynamic environment using a UCLA-developed HILSIM facility (see Figure 12). This facility runs a two-aircraft nonlinear model simulation and does not assume the availability of a reference ground station. An Interstate Electronics Corporation (IEC) two-frequency GPS Satellite Constellation Simulator (SCS) supplies the radio frequency (RF) GPS signals to the two receivers simulating the base and slave vehicles—FFIS 1 and FFIS 2—depending on their true trajectories, which are received in real-time. The two aircraft in the simulation are undergoing formation flight while moving at a velocity of approximately 180 m/s.

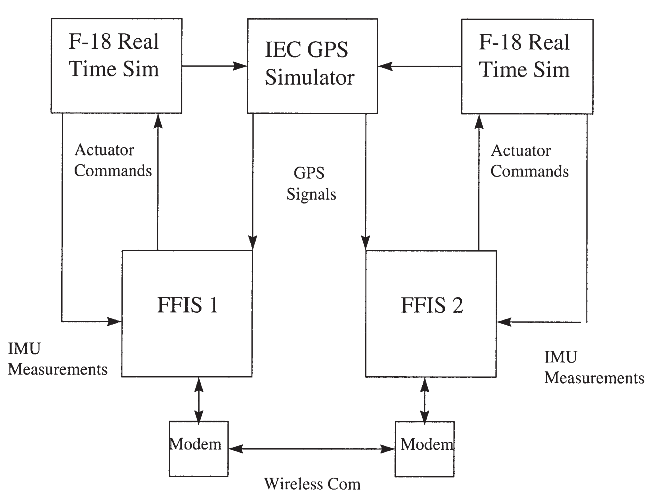

Fig. 12–UCLA Hardware-in-the-Loop Simulation Facility

Figure 13 presents real-time results for a dynamic 40 m baseline HILSIM experiment. The figure shows the probability associated with 10 integer hypotheses out of a total 100 hypotheses. The MHWSPT still converged to the true integer, in this case hypothesis 3. Because multipath GPS signal errors are not modeled, it can be seen that the probability of the correct hypothises continues to increase strictly as more GPS measurements are processed.

The baseline estimation error for the dynamic 40 m baseline HILSIM experiment is shown in Figure 14. In this experiment, the base and slave vehicles are flying in formation such that they remain around 40 m apart. Each aircraft is flying at about 180 m/s forward velocity. This testing environment was of great value in validating the performance of the algorithm because of the prior knowledge of the true trajectories of the base and slave vehicles. The figure indicates successful resolution of the integer ambiguity even in such a highly dynamic environment, as seen in the

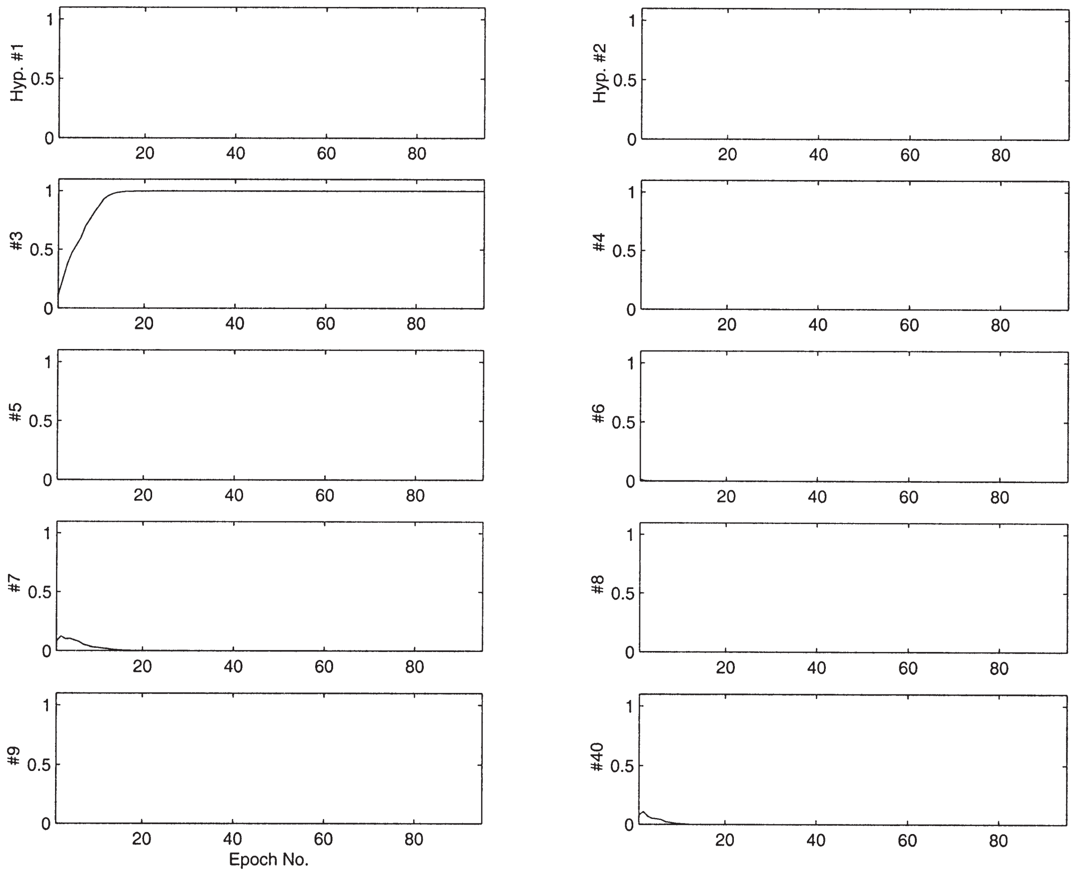

Fig. 13–MHWSPT Hypothesis Probabilities, Dynamic 40 m Baseline

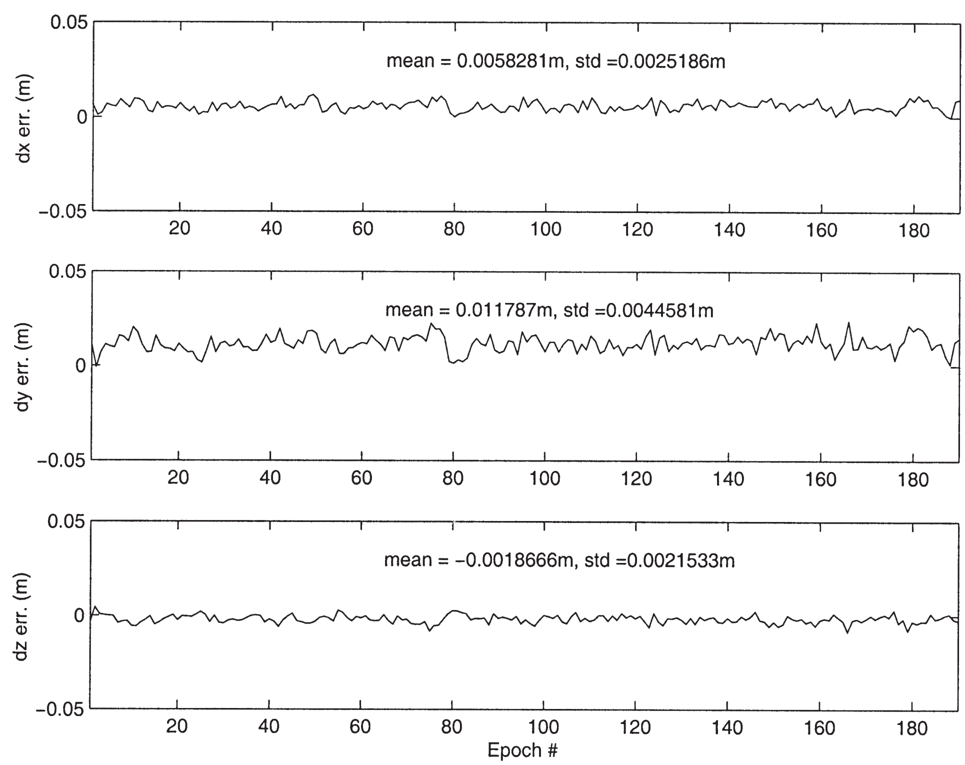

Fig. 14–Baseline Estimation Error after Fixing the Integers, 40 m Baseline Experiment

accurate relative position estimate of small error mean and standard deviation.

The ability of the proposed LAMBDA-assisted Wald test to resolve L1 integer ambiguity was also verified for all previous examples. Figures 15 and 16 present the results for the 40 m dynamic HILSIM experiment. Figure 15 shows the probability of the integer hypotheses being the correct integer ambiguity. It can be seen that processing the L1 GPS signal results only in a slower probability convergence speed. This result is expected since less information is being processed. It is also a consequence of the small L1 wavelength compared with the widelane wavelength. Therefore, the effect of GPS measurement noise on integer ambiguity resolution will be greater when the L1 integer ambiguity is being resolved than when the widelane integer ambiguity is being resolved. Despite the slower integer ambiguity convergence speed, however, L1 integer ambiguity resolution remains of interest to many researchers because of the low cost of L1 receivers compared with their dual-frequency counterparts.

Figure 16 shows the resulting relative position estimation accuracy after the L1 integer ambiguity has been resolved. It can be seen that when L1 GPS signals are used, the estimate deviation around the mean is small compared with the case in which widelane signals are used. This result is due to the added measurement noise when one is constructing the widelane measurement from the L1 and L2 GPS measurements.

Finally, the first column of Table 1 shows the central processing unit (CPU) computation time for the original MHWSPT, which assigned the integer hypotheses by offsetting ± 2 from each double-differenced measurement base hypothesis. The second column shows the CPU computation time used by the Kalman filter for the float solution and the LAMBDA decorrelation step. The third column shows the CPU computation time for the LAMBDA-assisted Wald test, which takes about 100 hypotheses that are enclosed by the ellipsoidal volume space of the covariance matrix. The algorithms were timed using a Linux Pentium III machine. It can be seen that the original MHWSPT takes considerably more time than the LAMBDA-assisted Wald test. This is because the number of hypotheses used by the original MHWSPT is 3,125 for six satellites, while the number for the LAMBDA-assisted Wald test is around 100. It can be also seen that the CPU computational time needed to run the LAMBDA decorrelation algorithm is small. Nevertheless, once the Kalman filter has converged, the LAMBDA decorrelation algorithm need be performed only once before the integer hypotheses in the ellipsoidal volume are efficiently determined. These hypotheses are then tested by the MHWSPT as GPS measurements are received until convergence on the correct integer ambiguity is achieved. It must again be emphasized that it is necessary to allocate enough time for the float Kalman filter to converge such that the resulting float estimate and its corresponding

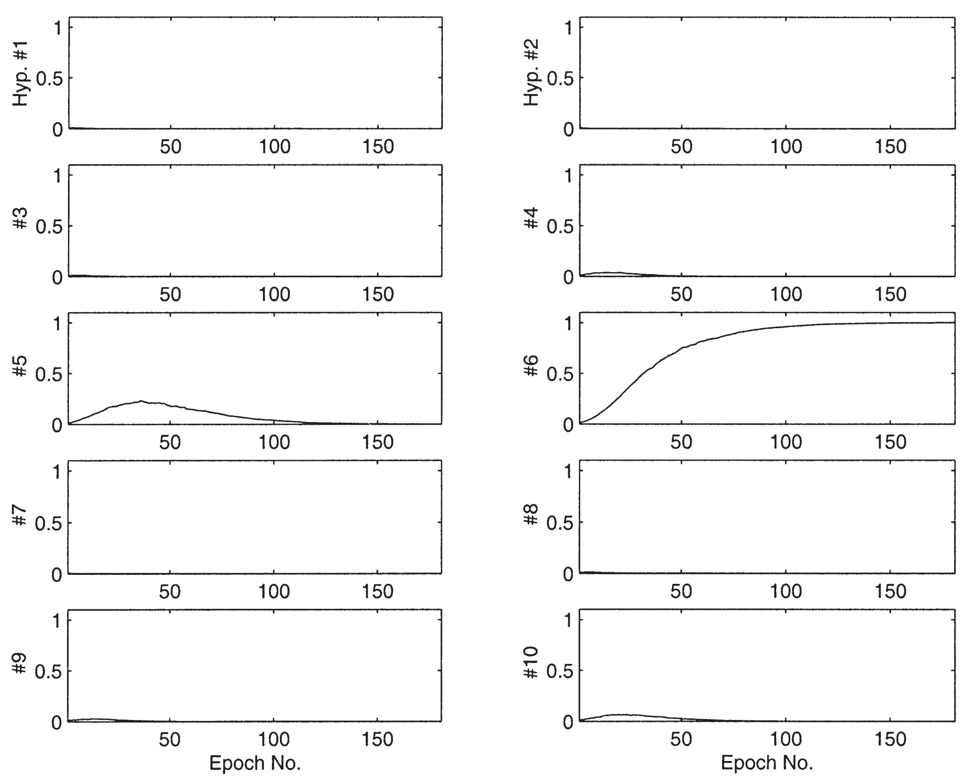

Fig. 15–MHWSPT Hypothesis Probabilities, Dynamic 40 m Baseline, L1 only

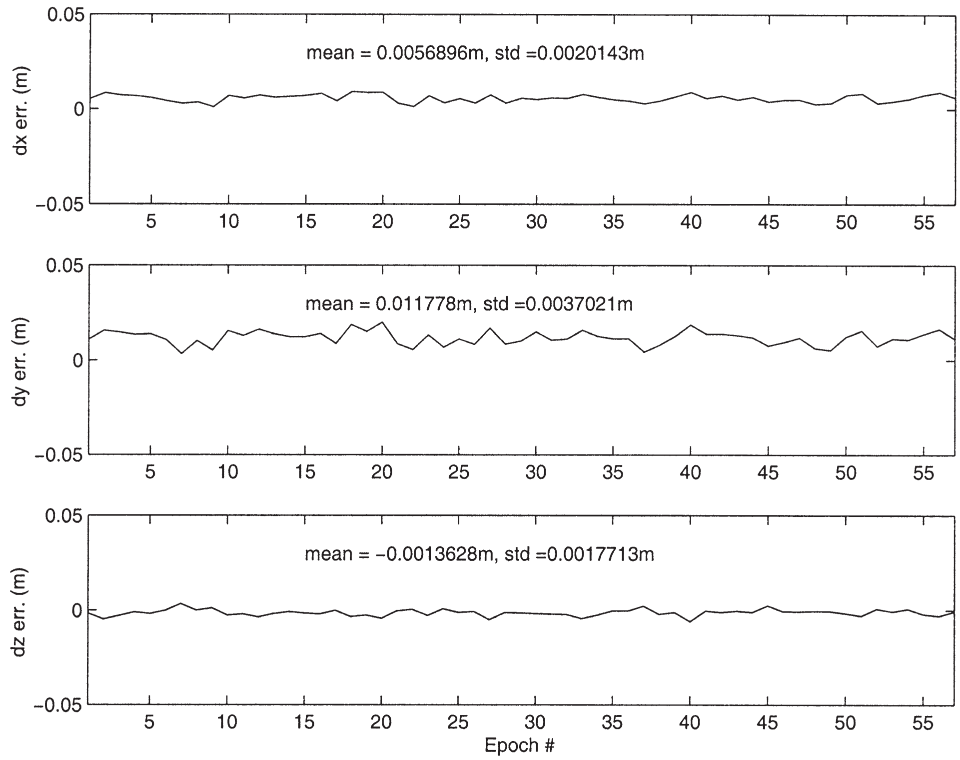

Fig. 16–Baseline Estimation Error after Fixing the Integers, 40 m Baseline Experiment, L1 only

Table 1—Computation Time Statistics (milliseconds)

Trial	Original MHWSPT	Kalman Filter and LAMBDA	LAMBDA-Assisted MHWSPT
1	21.932	3.597	0.424
2	21.866	3.588	0.429
3	21.902	3.593	0.424
4	22.331	3.590	0.423
5	21.886	3.606	0.424
6	21.944	3.589	0.430
7	22.077	3.599	0.429
8	21.883	3.600	0.433
9	22.953	3.593	0.426
10	21.878	3.592	0.426
Mean	22.0652	3.595	0.427

covariance matrix help define a compact hypothesis volume space that encloses the correct integer ambiguity.

CONCLUSIONS

A high-integrity and efficient method for GPS carrier-phase integer ambiguity resolution has been proposed. A Kalman filter that uses code, carrier-phase, and Doppler GPS measurements is first used to determine the float integer ambiguity and its corresponding covariance matrix. The method uses an efficient covariance matrix decorrelation algorithm to determine the integer hypotheses within a highly elongated covariance manifold. The hypotheses are then tested sequentially, and the probability of each hypothesis being the correct integer ambiguity is calculated recursively as new GPS measurements are sampled. An integer hypothesis is declared the correct hypothesis when its probability approaches 1. On the other hand, the probabilities of wrong hypotheses will approach zero. This new method is named the LAMBDA-assisted Wald test. Real-time results illustrating the accuracy and low computational time requirement of the method have been presented.

ACKNOWLEDGMENTS

This research was supported by NASA Ames under Grant No. NAG2-1484 and by NASA Goddard under Grant No. NAG5-11384.

Based on a paper presented at The Institute of Navigation's ION GPS-2002, Portland, Oregon, September 2002.

REFERENCES

1. Hatch, R. R., *Ambiguity Resolution in the Fast Lane,* Proceedings of The Institute of Navigation's ION GPS-89, 1989, pp. 45–50.
2. Hatch, R. R., *Ambiguity Resolution While Moving: Experimental Results,* Proceedings of The Institute of Navigation's ION GPS-91, 1991, pp. 707–13.

3. Min, J., *A Carrier Phase Differential Global Positioning System Algorithm for Relative State Estimation,* M.S. Thesis, UCLA, 1999, pp. 34–49.
4. Azimi-Sadjadi, B. and P. S. Krishnaprasad, *Integer Ambiguity Resolution in GPS Using Particle Filtering,* Proceedings of the American Control Conference, June 2001, pp. 3761–66.
5. Hassibi, A. and S. Boyd, *Integer Parameter Estimation in Linear Models with Applications to GPS,* IEEE Transactions on Signal Processing, Vol. 46, No. 11, 1998, pp. 2938–52.
6. Teunissen, P. J. G., *The Least Squares Ambiguity Decorrelation Adjustment: A Method for Fast GPS Integer Ambiguity Estimation,* Journal of Geodesy, Vol. 70(1–2), November 1995, pp. 65–83.
7. De Jonge, P. J. and C. C. J. M. Tiberius, *The LAMBDA Method for Integer Ambiguity Estimation: Implementation Aspects,* Publication of the Delft Geodetic Computing Center, Delft University of Technology, 1996.
8. Teunissen, P. J. G., P. J. De Jonge, and C. C. J. M. Tiberius, *Performance of the LAMBDA Method for Fast GPS Ambiguity Resolution,* NAVIGATION, Journal of The Institute of Navigation, Vol. 4, No. 3, 1997, pp. 373–83.
9. Malladi, D. P. and J. L. Speyer, *A Generalized Shiryayev Sequential Probability Ratio Test for Change Detection and Isolation,* IEEE Transactions on Automatic Control, Vol. 44, August 1999, pp. 1522–34.
10. Wald, A., *Sequential Analysis,* Wiley Mathematical Statistics Series, New York, NY, John Wiley and Sons, Inc., 1947.
11. Wolfe, J. D., W. R. Williamson, and J. L. Speyer, *Hypothesis Testing for Resolving Integer Ambiguity in GPS,* Proceedings of The Institute of Navigation's ION GPS-2001, September 2001, pp. 1522–31.
12. Maybeck, P. S., *Stochastic Models, Estimation and Control,* Vol. 1, Navtech Book and Software Store, 1994.
13. Park, C., I. Kim, J. G. Lee, and G. I. Lee, *Efficient Ambiguity Resolution Using Constraint Equations,* IEEE 1996 Position Location and Navigation Symposium—Plans 1996, IEEE, April 1996, pp. 277–84.